SINTEF
PROCEEDINGS 6

14th International Conference on CFD in
Oil & Gas, Metallurgical and Process Industries
SINTEF, Trondheim, Norway, October 12–14, 2020

Proceedings from the 14th International Conference on CFD in Oil & Gas, Metallurgical and Process Industries

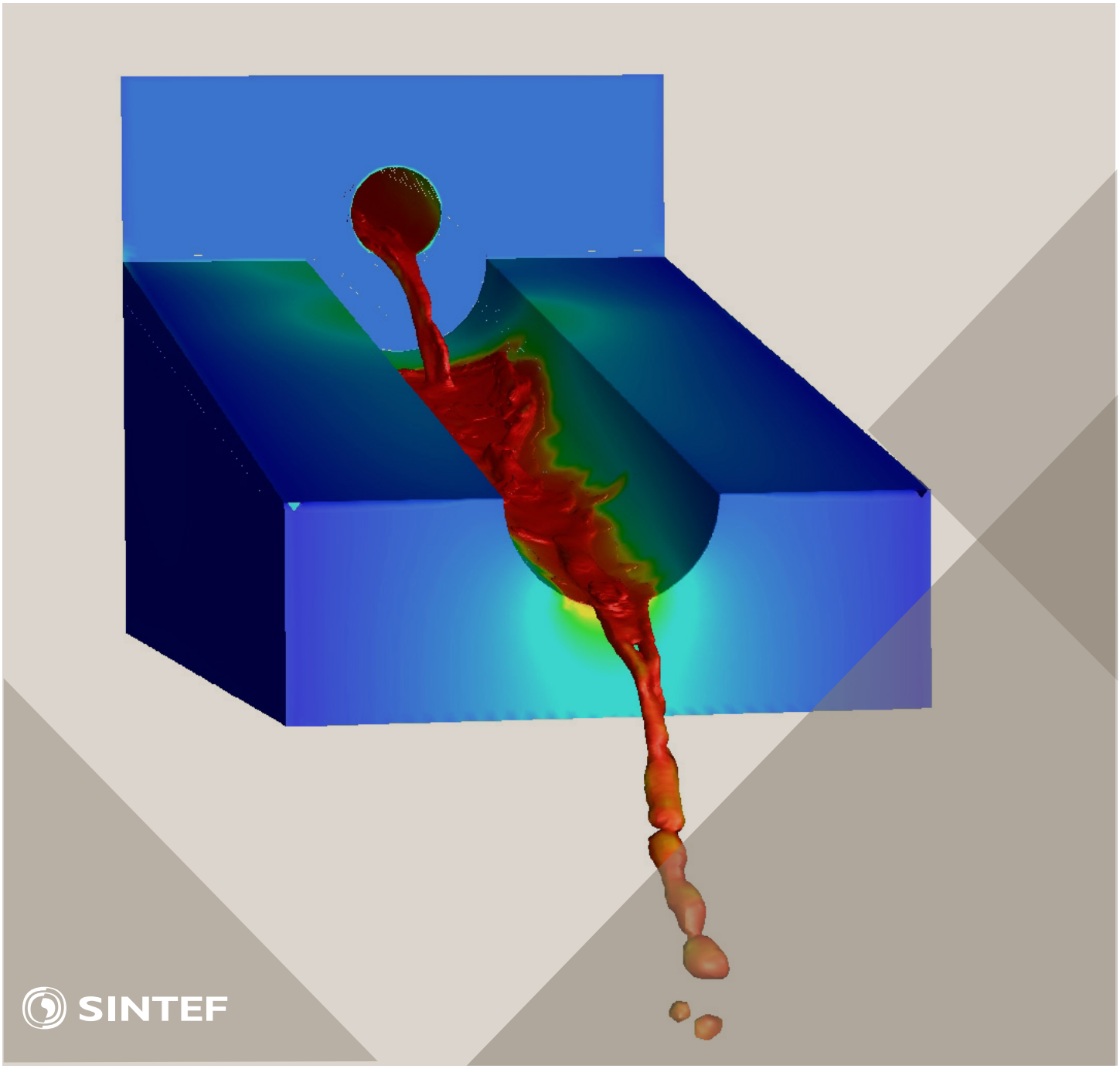

SINTEF Proceedings

Editors:
Jan Erik Olsen, Jan Hendrik Cloete and Stein Tore Johansen

Proceedings from the 14th International Conference on CFD in Oil & Gas, Metallurgical and Process Industries

SINTEF, Trondheim, Norway
October 12–14, 2020

SINTEF Academic Press

SINTEF Proceedings 6
Editors: Jan Erik Olsen, Jan Hendrik Cloete and Stein Tore Johansen

Proceedings from the 14th International Conference on CFD in Oil & Gas, Metallurgical and Process Industries, SINTEF, Trondheim, Norway, October 12–14, 2020

Keywords:
CFD, fluid dynamics, modelling

Cover illustration: Tapping of metal by Jan Erik Olsen

ISSN 2387-4295 (online)
ISBN 978-82-536-1684-1 (pdf)

SINTEF Academic Press
Address: Børrestuveien 3
PO Box 124 Blindern
N-0314 OSLO
Tel: +47 40 00 51 00

www.sintef.no/community
www.sintefbok.no

14th International Conference on CFD in Oil & Gas, Metallurgical and Process Industries
SINTEF, Trondheim, NORWAY
October 12-14, 2020

ON MODELLING ELECTROCHEMICAL GAS EVOLUTION USING THE VOLUME OF FLUID METHOD

Kurian J. VACHAPARAMBIL[1*], **Kristian Etienne EINARSRUD**[1†]

[1]Department of Materials Science and Engineering, Norwegian University of Science and Technology (NTNU), Trondheim 7491, Norway

[*] E-mail: kurian.j.vachaparambil@ntnu.no
[†] E-mail: kristian.e.einarsrud@ntnu.no

ABSTRACT

In this work we describe the various building block relevant in simulating electrochemical gas evolution using Volume of Fluid (VOF) method. These building blocks are implemented in the VOF solver available in OpenFOAM® and its predictions are compared to the theoretical models reported in literature. The fully coupled solver to model electrochemical gas evolution is used to model the case of a bubble evolving on a vertical electrode under constant potential condition to showcase its ability.

Keywords: VOF, Surface tension modelling, Interfacial mass transfer, Bubble growth, Gauss's law, Dissolved gas transport, Electrochemical systems .

NOMENCLATURE

Greek Symbols
ρ Density, $[kg/m^3]$
μ Dynamic viscosity, $[kg/ms]$
ν Kinematic viscosity, $[m^2/s]$
σ Surface tension, $[N/m]$
κ Interfacial curvature, $[1/m]$
α Volume fraction, $[-]$
ϕ Potential, $[V]$
β Growth coefficient, $[-]$
$\mathcal{F}$ Fraction of electrode area covered by bubble, $[-]$

Latin Symbols
D Diffusion coefficient, $[m^2/s]$.
$\vec{g}$ Acceleration due to gravity, $[m/s^2]$.
k Conductivity, $[S/m]$.
p Pressure, $[Pa]$.
C Molar concentration, $[mol/m^3]$.
$\vec{x}$ Position vector, $[m]$.
$\vec{U}$ Velocity vector, $[m/s]$.
$\vec{i}$ Current density vector, $[A/m^2]$.
$\vec{S}$ Individual cell face surface area vector, $[m^2]$.
He Jump condition across the interface, $[-]$.
f Void fraction, $[-]$.
R Bubble radius, $[m]$.
I Current when no bubbles are present, $[A]$.
d Interelectrode distance, $[m]$.
A Total electrode area, $[m^2]$.
M Molar mass, $[kg/mol]$.
F Faraday's constant (=96485), $[As/mol]$.

Sub/superscripts
1 Liquid or phase 1.
2 Bubble or phase 2.
i Dissolved gas species.
0 Operating condition.
s Saturation condition.
e Averaged or effective value.
$'$ Initial/starting condition.
m Modified.
∞ At bulk.
$\hat{}$ Harmonic average.

INTRODUCTION

Electrochemical gas evolution is relevant in a variety of industrial processes such as water-splitting, chloralkaline and Hall–Héroult. Bubble evolution in these systems involve nucleation, growth, coalescence and detachment from electrode. The dynamic behaviour of bubbles causes overpotential changes due to supersaturation, ohmic resistance and electrode screening, as well as enhanced mass transfer (Zhao *et al.*, 2019). Due to the complex and coupled nature of electrochemical gas evolution (Taqieddin *et al.*, 2018), numerical modelling of the system is an ideal way to understand its physics and develop strategies to efficiently remove these bubbles.

In literature, the numerical models used to simulate the continuum scale processes in electrochemical gas evolution can be broadly divided into dispersed and interface-resolving approaches. The dispersed approaches, like Euler-Euler, Mixture and Euler-Lagrange models, relies on a priori knowledge of flow to select interphase closure terms (Hreiz *et al.*, 2015). These approaches do not resolve the dispersed bubbles and are typically used to simulate industrial scale electrochemical systems (Hreiz *et al.*, 2015). On the other hand, interface-resolving approaches, like Volume of Fluid (VOF) (Einarsrud and Johansen, 2012; Einarsrud *et al.*, 2017; Sun *et al.*, 2018) and phase-field (Zhang *et al.*, 2020), resolve individual bubbles and is typically used to study in detail the dynamic behaviour of few bubbles. Although these studies have provided knowledge relevant to simulate the multiphysics nature of electrochemical gas evolution, there is still a lack research that addresses the coupled multiphysics as well as the multiscale nature of the process as highlighted by Taqieddin *et al.* (2018)

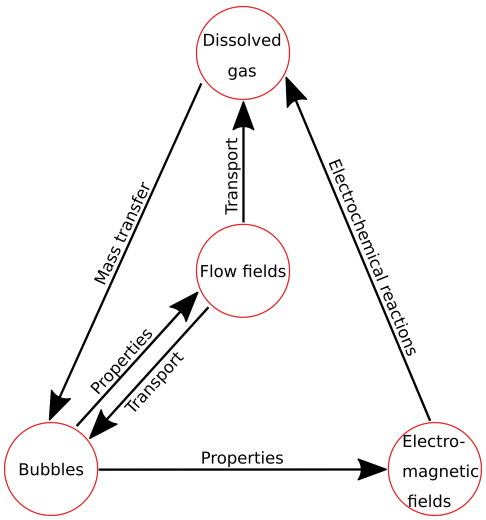

Figure 1: Schematic of the coupling between various modules of the proposed solver proposed to model electrochemical gas evolution.

In this work, we highlight various modules required to simulate electrochemical gas evolution, see Fig.1, to partly address the knowledge gap highlighted by Taqieddin *et al.* (2018). The decoupled modules are developed on the VOF solver available on OpenFOAM® 6, interFoam (Deshpande *et al.*, 2012). These modules are individually verified by comparison to relevant theoretical models available in literature and finally the potential of the fully coupled solver is discussed.

THE DECOUPLED MODEL DESCRIPTION

In this section, we introduce the various modules that are relevant in modelling electrochemical gas evolution: reliable small (sub-millimeter) bubbles, transport of dissolved gas, supersaturation driven bubble growth and ohmic resistance associated with bubble evolution. Before these individual modules are described, the VOF model as implemented in interFoam is introduced, for further details please refer Deshpande *et al.* (2012). The VOF model uses a scalar function known as volume fraction of liquid (α_1) which takes a value equal to unity in the liquid, zero in the gas phase and $0 < \alpha_1 < 1$ in the interface. The volume fraction of gas is calculated as $\alpha_2 = 1 - \alpha_1$. The advection of the volume fraction of liquid is computed as

$$\frac{\partial \alpha_1}{\partial t} + \nabla \cdot (\alpha_1 \vec{U}) + \nabla \cdot (\alpha_1(1-\alpha_1)\vec{U_r}) = 0, \quad (1)$$

where $\vec{U}$ is the velocity in domain and $\vec{U_r}$ is the compressive velocity computed based on a user-defined compression factor (C_α), see Deshpande *et al.* (2012). The fluid properties, like density (ρ) and viscosity (μ), are computed as $\chi = \alpha_1\chi_1 + \alpha_2\chi_2$. The mass conservation equation of the phases, described using continuity equation, is

$$\nabla \cdot \vec{U} = 0. \quad (2)$$

The momentum equation is written using a modified pressure, $p_m = p - \rho\vec{g} \cdot \vec{x}$, as

$$\frac{\partial \rho \vec{U}}{\partial t} + \nabla \cdot (\rho \vec{U}\vec{U}) = \nabla \cdot (\mu \nabla \vec{U}) + \nabla \vec{U} \cdot \nabla \mu + \vec{F}_{ST} - \nabla p_m - \vec{g} \cdot \vec{x} \nabla \rho, \quad (3)$$

where $\vec{F}_{ST}$ is the surface tension force is treated using the Continuum Surface Force (CSF) model (Brackbill *et al.*, 1992) and viscous term, usually written as $\nabla \cdot \mu(\nabla \vec{U} + \nabla \vec{U}^T)$ can be expressed as $\nabla \cdot (\mu \nabla \vec{U}) + \nabla \vec{U} \cdot \nabla \mu$ using Eq.2, see Deshpande *et al.* (2012).

Modelling sub-millimeter bubbles

One of the main well known problems associated with VOF approach is the errors in determining the local curvature used in surface tension modelling. These errors generate spurious velocities near the interface that can cause non-physical flow in the computational domain (Popinet, 2018; Vachaparambil and Einarsrud, 2019). The spurious velocities tend to become stronger with smaller length scales or lower Capillary number and it can sometimes be strong enough to generate nonphysical random walk of the bubbles. One of the approaches to reduce spurious velocities is to replace the commonly used CSF model with the Sharp Surface Force (SSF) model, proposed by Raeini *et al.* (2012), other advances has been reviewed in Popinet (2018). The work by Vachaparambil and Einarsrud (2019), has shown the ability of SSF to successfully simulate capillary rise and rising bubbles as well as reduce spurious velocities compared to CSF model.

The SSF model, based on the work of Raeini *et al.* (2012); Vachaparambil and Einarsrud (2019), describes $\vec{F}_{ST}$ as

$$\vec{F}_{ST} = \sigma \kappa_{final} \nabla \alpha_{sh}, \quad (4)$$

where κ_{final} is obtained using a three step smoothing of curvature and α_{sh} is calculated as

$$\alpha_{sh} = \frac{1}{1 - C_{sh}} \left[\min\left(\max\left(\alpha_1, \frac{C_{sh}}{2} \right), 1 - \frac{C_{sh}}{2} \right) - \frac{C_{sh}}{2} \right], \quad (5)$$

where C_{sh} is the user-defined sharpening coefficient which must satisfy $0 \leq C_{sh} < 1$. To model sub-millimeter bubble, the sharpening coefficient is set to 0.3 (Vachaparambil and Einarsrud, 2020b).

Transport of dissolved gas

Compared to single phase flows, the transport of species in a two phase flow requires the treatment of the interfacial conditions i.e. concentration jump across the interface and continuity of diffusive fluxes, see Maes and Soulaine (2018) or Deising *et al.* (2018). These interfacial conditions are incorporated into a single unified transport equation which solves for the concentration field in both liquid and the gas in the Compressive Continuous Species Transfer (CCST) model, developed by Maes and Soulaine (2018). The governing equation for C_i, in CCST model, is

$$\frac{\partial C_i}{\partial t} + \nabla \cdot (\vec{U} C_i) = \nabla \cdot (\hat{D}_i \nabla C_i - \hat{D}_i B C_i \nabla \alpha_1) - \nabla \cdot (B \alpha_1 \alpha_2 \vec{U}_r C_i), \quad (6)$$

where $\vec{U}_r$ is the compressive velocity (used in Eq.1), B is the defined as $(1 - He)/(\alpha_1 + \alpha_2 He)$, where He describes the concentration jump across the interface (also known as partition coefficient), and $\hat{D}_i$ is the harmonic averaging of the diffusion coefficients, see Maes and Soulaine (2018) for further details. Inorder to simulate the transport of dissolved

gas, which should only be in the liquid, we use He equal to a value near zero (like 10^{-4}), to minimize the transport of dissolved gas into the bubble which is accounted for by the CCST model based on the defined value of He (Maes and Soulaine, 2018; Vachaparambil and Einarsrud, 2020b). As He is a small number (10^{-4}), C_i obtained from Eq.6 can be interpreted as $C_i = \overline{C}_i - \overline{C}_s$, where $\overline{C}_i$ is the actual concentration and $\overline{C}_s$ represents the saturation concentration, based on Vachaparambil and Einarsrud (2020a,b).

Supersaturation driven bubble growth

When modelling interfacial mass transfer phenomena and the associated bubble growth, Sherwood number based correlations are widely used in CFD simulations (Einarsrud and Johansen, 2012; Einarsrud *et al.*, 2017). The drawback of these correlations is its limited applicability, due to its dependence on the bubble shape and relevant Reynolds and Schmidt number (Deising *et al.*, 2018). A more universal approach is to use the Fick's 1^{st} law, which is the governing equation used in deriving Sherwood number correlations (Bird *et al.*, 2007). To the best of the authors knowledge there are only two very recent works that has used Fick's 1^{st} law to model bubble evolution: Vachaparambil and Einarsrud (2020a,b) and Maes and Soulaine (2020).

In order to model the growth of bubble driven by the supersaturated electrolyte, we use the approach proposed by Vachaparambil and Einarsrud (2020a,b). In this work, the phenomenological Fick's 1^{st} law, the driving force for bubble growth, is coupled to CCST, described based on Eq.6, with relevant source terms for species transport (Eq.6), advection of α_1 (Eq.1) and continuity (Eq.2) equations is implemented by extending the work of Hardt and Wondra (2008). For information about the relevant governing equations and source terms, please refer to Vachaparambil and Einarsrud (2020b).

Modelling electromagnetic effects

To model the electromagnetic effects, we use Gauss's law which can be described mathematically as

$$\nabla \cdot \vec{i} = 0, \tag{7}$$

where the current density ($\vec{i}$) can be expressed using the gradient of potential (ϕ) as

$$\vec{i} = -k\nabla\phi, \tag{8}$$

where k is the conductivity, calculated as an algebraic averaging of conductivities, i.e. $\alpha_1 k_1 + \alpha_2 k_2$. This approach has been used in literature to describe the evolution of carbon dioxide bubbles in aluminum reduction process (Einarsrud and Johansen, 2012).

SOLVER SETTINGS

Due to the coupled nature of momentum and pressure equations, the equations are computed using the PISO algorithm, see Deshpande *et al.* (2012). The governing equations are discretized with first order schemes for time and second order schemes in space, for details please refer to Vachaparambil and Einarsrud (2020b). The convergence criterion used solve governing equations for p_{rgh} and other variables (like ϕ, $\vec{U}$, C_i and others) are 10^{-20} and 10^{-10} respectively. When surface tension is relevant in the simulations, a constraint on time step constraint described in Deshpande *et al.* (2012); Vachaparambil and Einarsrud (2019) is used to prevent the growth of spurious velocities.

VERIFICATION OF THE DECOUPLED SOLVER

In this section, we verify the individual modules implemented in interFoam using theoretical models described in literature.

On sub-millimeter bubbles

The ability of the SSF model to reliably simulate sub-millimeter bubbles is demonstrated by a simulation of a stationary bubble. Without body forces, i.e. gravity, in the domain, any velocities present in the simulation can be attributed to spurious velocities. As electrochemically generated bubbles can be present on both the electrode surface and in the bulk (after detachment), it is necessary to reliably simulate sub-millimeter bubbles for both cases.

The properties of the liquid and gas used in the simulation are $\rho_1 = 1000\text{kg/m}^3$, $\rho_2 = 1\text{kg/m}^3$, $\nu_1 = 10^{-6}\text{m}^2\text{/s}$, $\nu_2 = 1.48\times10^{-5}\text{m}^2\text{/s}$ and $\sigma = 0.07\text{N/m}$. Two test cases, where the bubble is available in the bulk (SBC1) and attached to the electrode surface (SBC2), where the stationary bubble has a diameter ($2R$) of 0.5mm are simulated in a 2D domain of dimensions $4R \times 4R$. Both SBC1 and SBC2 are meshed using a hexahedral grid with 120×120 cells. For SBC1, all the boundaries are assigned zeroGradient for both $\vec{U}$ and α_1 but the p_{rgh} is assigned fixedValue of 101325Pa. In the case of SBC2, where the left and right boundaries are defined as walls, $\vec{U}$ uses no-slip condition at the walls and zeroGradient at the other boundaries along with α_1 uses zeroGradient on all boundaries (with a default contact angle of 90° at the walls) and p_{rgh} as fixedValue (equal to 0Pa) at the top wall and fixedFluxPressure (Greenshields, 2019) on the other boundaries. Due to the surface tension, the maximum time step allowed is manually limited to 0.6μs (see Deshpande *et al.* (2012); Vachaparambil and Einarsrud (2019)) and the simulations are run until 0.05s.

The accuracy of these simulations are estimated using Laplace pressure and magnitude spurious velocities, like in Vachaparambil and Einarsrud (2019). The Laplace pressure in a 2D bubble can be calculated based on Young-Laplace equation as $\Delta p_c = \sigma/R$ and the spurious velocities (U_{sc}) is estimated as max($|\vec{U}|$). The Laplace pressure in the bubble, from the simulations, is calculated as

$$\Delta p = \frac{\int_V \alpha_2 p dV}{\int_V \alpha_2 dV} - p_0, \tag{9}$$

where p_0 is the operating pressure used in the simulations. The associated error in Laplace pressure (E) is calculated as $(\overline{\Delta p} - \Delta p_c)/\Delta p_c$, where the overbar indicates the averaged value over the simulation time.

Table 1: Time averaged values of spurious velocities, Laplace pressure and its error obtained while simulating a stationary sub-millimeter bubble.

Case	$\overline{U_{sc}}$ (m/s)	$\overline{\Delta p}$ (Pa)	E
SBC1	0.0108	255.35	−0.088
SBC2	0.0198	253.91	−0.093

As shown in Fig.2, the spurious velocities generated are present on both sides of the interface (for both TC1 and

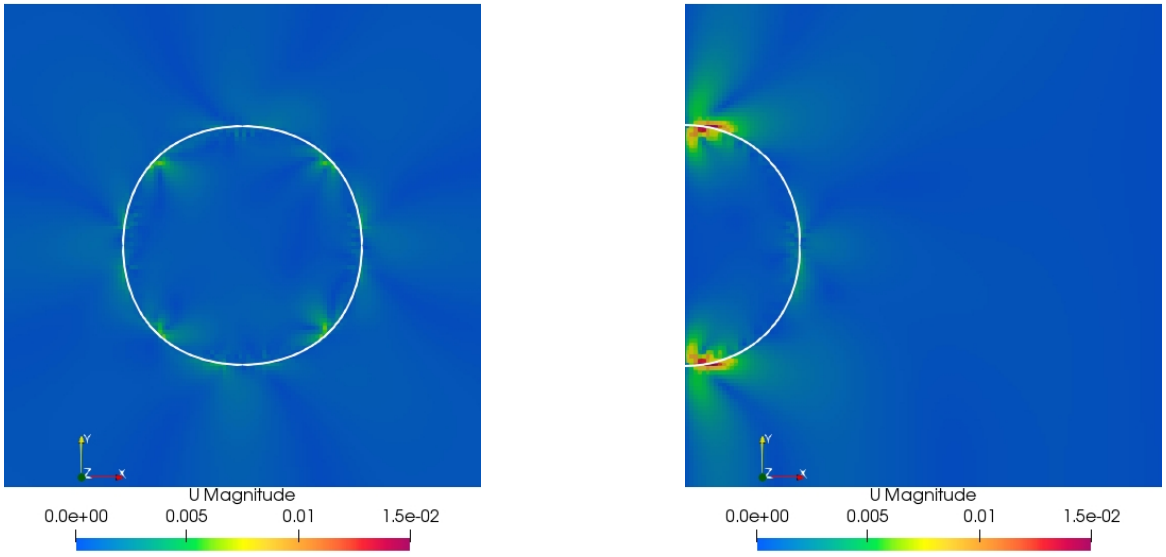

(a) Bubble in the bulk (SBC1).

(b) Bubble on the wall (SBC2).

Figure 2: Comparison of the spurious velocities (m/s) generated while modelling stationary bubbles at $t = 0.05$s with interface (at $\alpha_1 = 0.5$) represented by the white contour.

TC2). Interestingly, the spurious velocities generated are quite different in both TC1 and TC2, with the latter generating strong spurious velocities near the foot of the bubble. These time averaged spurious velocities and error in estimating the Laplace pressure of the bubble quantified in Table.1.

On the transport of dissolved gas

In order to show that Eq.6 with $He = 10^{-4}$ can model the transport of dissolved gas reasonably well, we take a hypothetical case where a rising bubble moves through a region of supersaturation. The fluid properties used in the simulations, which are adapted from Hysing *et al.* (2009), are $\rho_1 = 1000\text{kg/m}^3$, $\rho_2 = 1\text{kg/m}^3$, $\nu_1 = 0.01\text{m}^2\text{/s}$, $\nu_2 = 0.1\text{m}^2\text{/s}$, $\sigma = 1.96\text{N/m}$ and $|\vec{g}| = 0.98\text{m/s}^2$ along with $D_1 = 10^{-9}\text{m}^2\text{/s}$ and $D_2 = 10^{-5}\text{m}^2\text{/s}$. A bubble of diameter 0.5m is initialized such that its center is 0.5m from the bottom and side boundaries in a domain of dimensions 1m×2m. The simulation is run with hexahedral mesh with 160×320 cells. The region of supersaturation, $C_i = 10\text{mol/m}^3$, is initialized in an area of 1m×0.7m from a distance of 0.8m from the bottom wall. All four boundaries are assigned the zeroGradient condition for C_i and α_1. The boundary conditions for $\vec{U}$ are assigned slip conditions at the side walls and remaining walls are set as no-slip. For p_{rgh}, the top wall is assigned the fixedValue (equal to zero) but the other walls are described using fixedFluxPressure (Greenshields, 2019).

The spatial distribution of the dissolved gas as the bubble rises and deforms is illustrated in Fig.3. The convection induced by the rising bubble does not advect the dissolved gas into the bubble. Due to the use of a non-zero He, to prevent B in Eq.6 from becoming infinity, dissolved gas does numerically drift into the bubble but this is negligible (lower than 0.01% of the amount of dissolved gas).

On supersaturation driven bubble growth

Adapted fromVachaparambil and Einarsrud (2020a,b), the fluid properties used in the simulation are $\rho_1 = 997.08\text{kg/m}^3$, $\rho_2 = 1.81\text{kg/m}^3$, $\nu_1 = 8.92 \times 10^{-7}\text{m}^2\text{/s}$, $\nu_2 = 8.228 \times 10^{-6}\text{m}^2\text{/s}$, $D_1 = 1.94 \times 10^{-9}\text{m}^2\text{/s}$, $D_2 = 9.18 \times 10^{-6}\text{m}^2\text{/s}$ and $M = 44 \times 10^{-3}\text{kg/mol}$. Both surface tension and gravity are neglected in the simulations. The parameters used in the solver are defined based on the work by Vachaparambil and Einarsrud (2020b). The domain used for the computation is 3cm×3cm which is meshed with 4000×4000 cells, the pre-existing bubble (of diameter equal to 0.5mm) is initialized at the center of the domain. The liquid phase is initialized with a concentration of dissolved gas at 200.64mol/m^3. The boundary conditions used are described in Vachaparambil and Einarsrud (2020b).

The approach to describe the growth of a pre-existing bubble in a supersaturated solution can be verified by the Extended Scriven model proposed by Hashemi and Abedi (2007) (based on the work by Scriven (1959)):

$$R = 2\beta\sqrt{D_1\left(t + \frac{R'^2}{4D_1\beta^2}\right)}, \tag{10}$$

where β is the growth coefficient and R' is the radius of the pre-existing bubble. The growth coefficient for 2D bubbles, derived in Vachaparambil and Einarsrud (2020b), is

$$\beta_{2D} = \frac{a + \sqrt{a^2 + 4a}}{2\sqrt{2}}, \tag{11}$$

where a is equal to $M\Delta C/\rho_2$ and ΔC is equal to the concentration of the dissolved gas that is over the saturation condition (equal to 200.64mol/m^3). Fig.4 shows that the evolution of bubble radius predicted by the model agrees reasonably with the Extended Scriven with β_{2D}. The discrepancy between the simulation and the Extended Scriven model can be explained by the discontinuous nature of dissolved gas concentration at $t = 0$s (Vachaparambil and Einarsrud, 2020a,b).

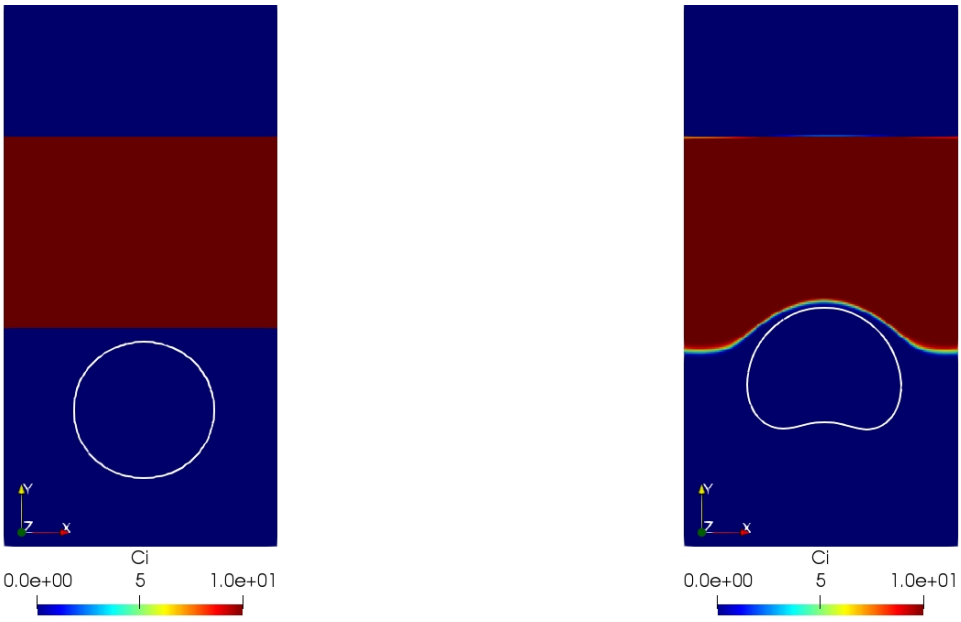

(a) $t = 0$s. **(b)** $t = 1$s. **(c)** $t = 2$s. **(d)** $t = 3$s.

Figure 3: The concentration of dissolved gas (mol/m^3) around a rising bubble (interface, at $\alpha_1 = 0.5$, is represented by white contour) modelled based on Eq.6.

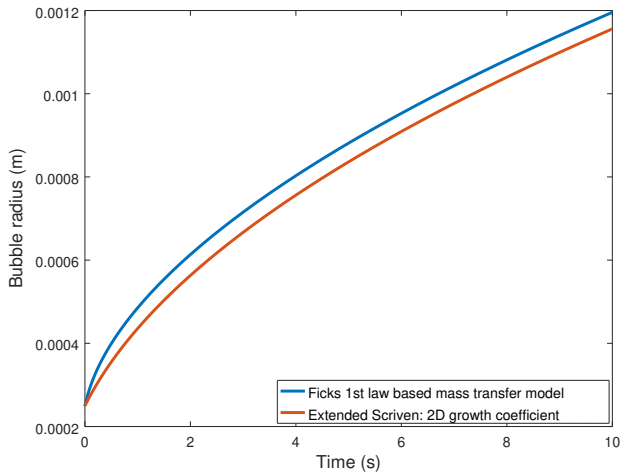

Figure 4: Comparison of the bubble growth predicted by Fick's 1^{st} law based model (based on the work by Vachaparambil and Einarsrud (2020b)) and the the Extended Scriven model (Eq.10) using $\beta_{2D} = 4.0509$.

On electromagnetism and its effects

In the case of constant potential difference across the electrodes, the current varies due to the bubble evolution. The effect of bubbles can be divided based on its position, i.e. in the bulk and attached to the electrode, which is investigated in this subsection.

The fluid parameters used for these simulations are $\rho_1 = 1000\text{kg/m}^3$, $\rho_2 = 1\text{kg/m}^3$, $\nu_1 = 10^{-6}\text{m}^2\text{/s}$, $\nu_2 = 1.48 \times 10^{-5}\text{m}^2\text{/s}$, $k_1 = 100\text{S/m}$ and $k_2 = 10^{-13}\text{S/m}$. Both gravity and surface tension are neglected in these simulations. Assuming that the electrolyte is bubble free, for an inter-electrode gap of 1cm and the difference in potential between the electrode is 0.01V corresponds to a current density of 100A/m^2. Any change in current density can be attributed to the presence of bubbles in the computational domain.

When bubbles are attached on the electrode surface

When bubbles are present on the electrode surface, it increases the resistance in the system due to volume of the bubble and electrode screening. If an area of 2D bubble, which is present in the bulk, is redistributed on the surface such that the effective area is the same, the current reduces due to the increase in effective resistance at the electrode (due to electrode screening). This is showcased by considering two cases: EC1 (bubble is present in the bulk) and EC2 (bubble is attached to the electrode), see Fig.5.

The computational domain, of dimensions 1cm×1cm, is meshed by 200×200 cells. The left and right boundaries, which are the electrodes, are assigned as no-slip conditions for velocity and fixedFluxPressure (Greenshields, 2019) for pressure. The top and bottom boundaries are assigned fixedValue (equal to 0Pa) for p_{rgh} and zeroGradient for velocity. All the boundaries are assigned zeroGradient for α_1. For ϕ, left and right walls are assigned 0V and 0.01V respectively, whereas the remaining boundaries are set as zeroGradient. The initial conditions for the α_1, are set as described in Fig.5.

The reduction of the current due to the presence of the bubble on the electrode surface is shown in Table.2.

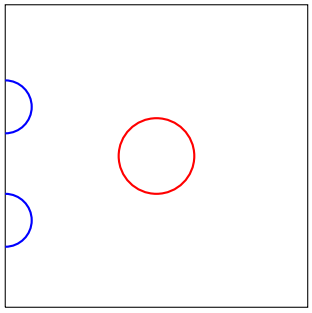

Figure 5: Illustration of the cases, EC1 and EC2, considered to showcase the effect electrode screening. EC1, represented by ━, considers a bubble of radius 1mm at the center of domain. EC2, represented by ━, considers two equally sized bubbles (semicircles with radii equal to 1mm) whose centers are 2.5mm and 6.5mm away from the bottom wall.

Table 2: Reduction of current due to the presence of bubble on the electrode.

Case	$\mathcal{F}^a$	Area of 2D bubbles (m^2)	Current^b (A)
EC1	1	3.16×10^{-6}	9.384×10^{-7}
EC2	0.6	3.16×10^{-6}	9.306×10^{-7}

^{a} $\mathcal{F}$ represents the fraction of the left electrode area in contact with electrolyte, ^{b} Current is calculated as $\sum \vec{i}.\vec{S}$ where $\vec{S}$ is the face surface area of individual cell on the left electrode.

When bubbles are present in the bulk

The 2D simulations use the a domain, of size 1cm×1cm, which is meshed with 200×200 cells. The left and right boundaries use no-slip, fixedFluxPressure (Greenshields, 2019) and fixedValue (equal to 0V and 0.01V) for $\vec{U}$, p_{rgh} and ϕ respectively. The other boundaries are assigned zeroGradient for both $\vec{U}$ and ϕ whereas p_{rgh} use fixedValue (equal to 0V). For α_1, all the boundaries are assigned the zeroGradient condition. For 3D simulations, the domain of size 1cm×1cm×1cm is meshed with 200×200×200 cells. The left and right boundaries are set according to the analogous conditions for 2D simulations whereas the remaining boundaries are treated like the top/bottom boundaries used in 2D simulations. The initial conditions used for α_1 is chosen so that bubble, with a range of sizes, are randomly placed in the bulk, as shown in Fig.A1 and Fig.A2 for 2D and 3D simulations respectively.

The bubbles change the effective conductivity of the electrolyte (k_e) which can be theoretically estimated using the Bruggermann's correlation (valid for polydispersed spherical bubbles (Bruggeman, 1935)) as

$$k_e/k_1 = (1 - f)^{1.5}, \tag{12}$$

where f is the void fraction (calculated as the ratio of total volume of the bubble to the volume of the domain). Once the k_e is computed, the resistance is computed as $d/(k_e A)$, where d is the interelectrode distance (equal to 1cm) and A is the area of the 3D electrode (equal to $0.01 \times 0.01\text{m}^2$), and current in the system and current density are determined based on Ohm's law with cell voltage computed as the difference between the right and left boundary conditions for ϕ (equal to 0.01V). As expected, Fig.6 shows that 3D simulations provides a better agreement to the current density obtained from Bruggermann correlations than the 2D simulations. Further the solver successfully predicts the

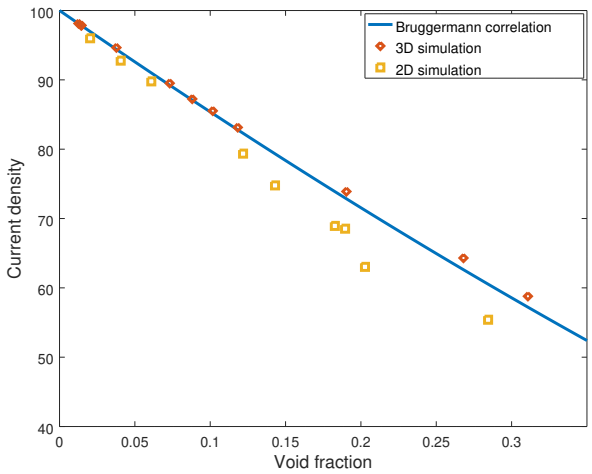

Figure 6: Comparison of the current density (A/m^2) reduction with increase in void fraction of bubbles (in bulk) predicted by the simulations (for 2D and 3D) and Bruggermann's correlation.

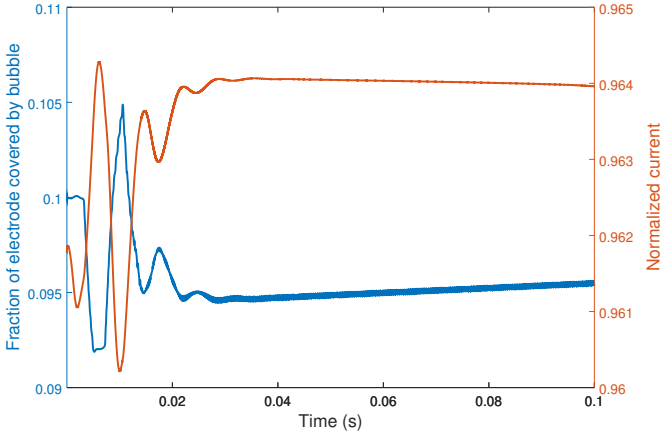

Figure 8: Comparison change in footprint of the bubble on the electrode (fraction of bubble covered electrode) and the associated change in normalized current (calculated as $(\sum \vec{i} \cdot \vec{S})/(I)$, where I is the current when no bubbles are present, i.e. 100A/m^2 $\times(5\times10^{-9}\text{m}^2)$) with time.

reduction of current density with the increase in the void fraction of bubbles.

ON THE FULLY COUPLED SOLVER

For the fully coupled solver, the solution is obtained by solving the volume fraction equation, then calculating the relevant source terms, the coupled momentum and continuity equations, then the Gauss'law and finally the transport of dissolved gas using CCST model at each time step.

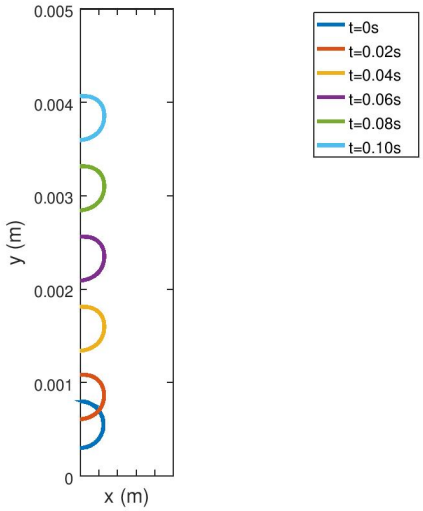

Figure 7: Comparison interface morphology and position with time in the computational domain.

In order to showcase the ability of the solver, we simulate the growth of a pre-existing bubble due to electrochemical reactions occurring at a vertical electrode-electrolyte interface. The occurrence of pre-existing bubbles at surface imperfections, for instance from previous nucleation events, can reduce the energy required for nucleation to values as low as zero (Vachaparambil and Einarsrud, 2018). This approximation, which is physically reasonable as bubble has been observed to generate from the same site on the electrode for a range of current densities (Westerheide and Westwater, 1961; bo Liu *et al.*, 2019), enables direct modelling of the growth of the bubble without the need to treat bubble nucleation. In order to treat bubble nucleation in a CFD framework, algorithms like the one proposed by Damme *et al.* (2010) are required.

The computational domain used for the simulation is 1mm$\times$5mm which is meshed by 200$\times$1000 cells. The left and right boundaries are set as walls and the boundary conditions are described based on the individual modules in the decoupled solver except for the the C_i at the left wall which is computed using the Faraday's law of electrolysis, as $\partial_n C_i = |\vec{i}|\alpha_1/(2FD_1)$, and ϕ is assigned a fixedValue of 0V and 10^{-3}V at left and right walls respectively. The pre-existing bubble, of radius equal to 0.25mm, is initialized as that its center is on the left wall at a distance of 0.55mm from the lower boundary. The fluid properties used in the proof of concept simulation are: $\rho_1 = 1000\text{kg/m}^3$, $\rho_2 = 1\text{kg/m}^3$, $\nu_1 = 10^{-6}\text{m}^2/\text{s}$, $\nu_2 = 1.48\times10^{-5}\text{m}^2/\text{s}$, $D_1 = 10^{-9}\text{m}^2/\text{s}$, $D_2 = 10^{-5}\text{m}^2/\text{s}$, $\sigma = 0.003\text{N/m}$, $M = 44\times10^{-3}\text{kg/mol}$, $k_1 = 100\text{S/m}$, $k_2 = 10^{-13}\text{S/m}$ and $|\vec{g}| = 9.81\text{m/s}^2$. Due to the use of surface tension, the maximum time step allowed is manually limited to 8μs (see Deshpande *et al.* (2012); Vachaparambil and Einarsrud (2019)) and the simulations are run until 0.1s.

The concentration distribution of the dissolved gas generated by the electrochemical reactions and the current density distribution around the rising bubble attached to the electrode at $t = 0.1$s is shown in Fig.9. As the bubble rises up, the growth rate and the effective radius of the bubble increases as seen in Fig.10 which is associated with the increase in the bubble footprint after the initial transient behaviour of the bubble, see Fig.8. The change in current obtained directly correlates with the footprint and size of the bubble, see Fig.8 and Fig.10.

CONCLUSION

We implemented the individual models relevant in modelling an electrochemical gas evolution in the VOF solver available in OpenFOAM® 6. The modules added into interFoam are: SSF (for surface tension modelling), C-CST

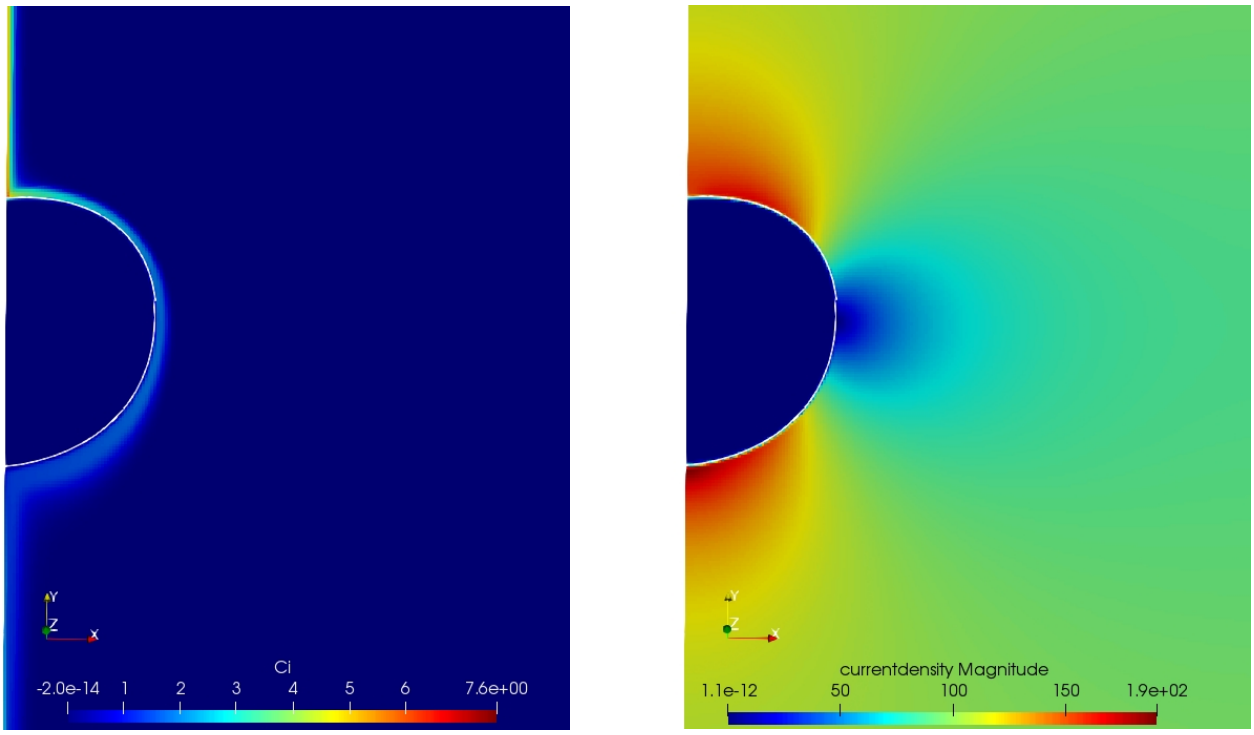

(a) C_i (mol/m^3). **(b)** $|\vec{i}|$ (A/m^2).

Figure 9: Comparison of the distribution of dissolved gas and current density (magnitude) around the bubble (whose interface, at $\alpha_1 = 0.5$, is represented by the white contour) at $t = 0.1$s.

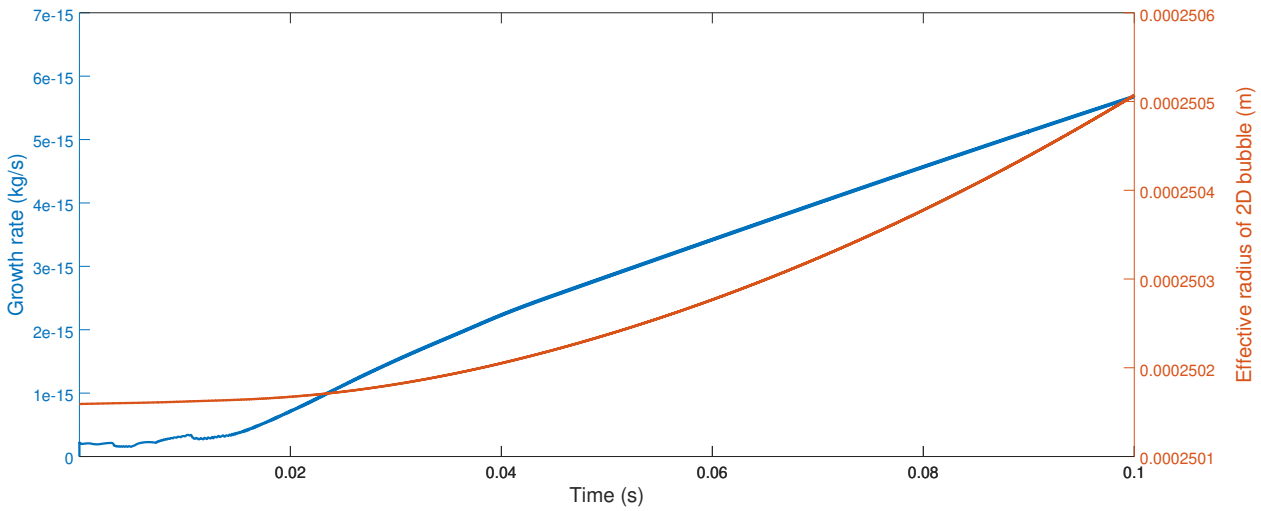

Figure 10: Comparison of the growth rate and the effective radius of the bubble as it evolves.

(transport of dissolved gas), supersaturation driven bubble growth model and Gauss's law. The predictions from these decoupled modules agree quite reasonably with relevant theoretical models available in literature. The bubble evolution, under constant potential condition, as predicted by the fully coupled solver is also discussed to showcase the ability of the proposed solver to handle electrochemical gas evolution. The proposed fully coupled solver, unlike other works reported in literature, can 'theoretically' be applied to simulate a variety of flow configuration (current density and electrode orientations) as well as the impact of bubble detachment in electrochemical systems due to the use of phenomenological models.

ACKNOWLEDGEMENTS

This work was funded by the Department of Materials Science and Engineering at NTNU. The authors would also like to thank UNINETT Sigma2 for providing necessary computational resources through grant NN9741K.

REFERENCES

BIRD, R., STEWART, W. and LIGHTFOOT, E. (2007). *Transport Phenomena: Revised Second Edition*. Wiley, New York.

BO LIU, H., HU, Q., MING PAN, L., WU, R., LIU, Y. and ZHONG, D. (2019). "Electrode-normal magnetic field facilitating neighbouring electrochemical bubble release from hydrophobic islets". *Electrochimica Acta*, **306**, 350 – 359.

BRACKBILL, J., KOTHE, D. and ZEMACH, C. (1992). "A continuum method for modeling surface tension". *Journal of Computational Physics*, **100(2)**, 335 – 354.

BRUGGEMAN, D.A.G. (1935). "Berechnung verschiedener physikalischer konstanten von heterogenen substanzen. i. dielektrizitätskonstanten und leitfähigkeiten der mischkörper aus isotropen substanzen". *Annalen der Physik*, **416(7)**, 636–664.

DAMME, S.V., MACIEL, P., PARYS, H.V., DECONINCK, J., HUBIN, A. and DECONINCK, H. (2010). "Bubble nucleation algorithm for the simulation of gas evolving electrodes". *Electrochemistry Communications*, **12(5)**, 664 – 667.

DEISING, D., BOTHE, D. and MARSCHALL, H. (2018). "Direct numerical simulation of mass transfer in bubbly flows". *Computers & Fluids*, **172**, 524 – 537.

DESHPANDE, S.S., ANUMOLU, L. and TRUJILLO, M.F. (2012). "Evaluating the performance of the two-phase flow solver interFoam". *Computational Science & Discovery*, **5(1)**, 014016.

EINARSRUD, K.E. and JOHANSEN, S.T. (2012). "Modelling of bubble behaviour in aluminium reduction cells". *Progress in Computational Fluid Dynamics, an International Journal*, **12(2-3)**, 119–130.

EINARSRUD, K.E., EICK, I., BAI, W., FENG, Y., HUA, J. and WITT, P.J. (2017). "Towards a coupled multi-scale, multi-physics simulation framework for aluminium electrolysis". *Applied Mathematical Modelling*, **44**, 3 – 24.

GREENSHIELDS, C.J. (2019). "Openfoam user guide version 7". URL `http://foam.sourceforge.net/docs/Guides-a4/OpenFOAMUserGuide-A4.pdf`.

HARDT, S. and WONDRA, F. (2008). "Evaporation model for interfacial flows based on a continuum-field representation of the source terms". *Journal of Computational Physics*, **227(11)**, 5871 – 5895.

HASHEMI, S.J. and ABEDI, J. (2007). "Advances in modeling of new phase growth". *Energy & Fuels*, **21(4)**, 2147–2155.

HREIZ, R., ABDELOUAHED, L., FÜNFSCHILLING, D. and LAPICQUE, F. (2015). "Electrogenerated bubbles induced convection in narrow vertical cells: A review". *Chemical Engineering Research and Design*, **100**, 268 – 281.

HYSING, S., TUREK, S., KUZMIN, D., PAROLINI, N., BURMAN, E., GANESAN, S. and TOBISKA, L. (2009). "Quantitative benchmark computations of two-dimensional bubble dynamics". *International Journal for Numerical Methods in Fluids*, **60(11)**, 1259–1288.

MAES, J. and SOULAINE, C. (2018). "A new compressive scheme to simulate species transfer across fluid interfaces using the volume-of-fluid m ethod". *Chemical Engineering Science*, **190**, 405 – 418.

MAES, J. and SOULAINE, C. (2020). "A unified single-field v olume-of-fluid-based fo rmulation fo r multi-component interfacial transfer with local volume changes". *Journal of Computational Physics*, **402**, 109024.

POPINET, S. (2018). "Numerical models of surface tension". *Annual Review of Fluid Mechanics*, **50(1)**, 49–75.

RAEINI, A.Q., BLUNT, M.J. and BIJELJIC, B. (2012). "Modelling two-phase flow i n p orous m edia a t t he pore scale using the volume-of-fluid m ethod". *Journal of Computational Physics*, **231(17)**, 5653 – 5668.

SCRIVEN, L. (1959). "On the dynamics of phase growth". *Chemical Engineering Science*, **10(1)**, 1 – 13.

SUN, M., LI, B. and LI, L. (2018). "A multi-scale mathematical model of growth and coalescence of bubbles beneath the anode in an aluminum reduction cell". *Metallurgical and Materials Transactions B*, **49(5)**, 2821–2834.

TAQIEDDIN, A., ALLSHOUSE, M.R. and ALSHAWABKEH, A.N. (2018). "Editors' choice—critical review—mathematical formulations of electrochemically gas-evolving systems". *Journal of The Electrochemical Society*, **165(13)**, E694–E711.

VACHAPARAMBIL, K.J. and EINARSRUD, K.E. (2018). "Explanation of bubble nucleation mechanisms: A gradient theory approach". *Journal of The Electrochemical Society*, **165(10)**, E504–E512.

VACHAPARAMBIL, K.J. and EINARSRUD, K.E. (2019). "Comparison of surface tension models for the volume of fluid m ethod". *Processes*, **7(8)**, 542.

VACHAPARAMBIL, K.J. and EINARSRUD, K.E. (2020a). "Modeling interfacial mass transfer driven bubble growth in supersaturated solutions". *AIP Advances*, **10(10)**, 105024.

VACHAPARAMBIL, K.J. and EINARSRUD, K.E. (2020b). "Numerical simulation of bubble growth in a supersaturated solution". *Applied Mathematical Modelling*, **81**, 690 – 710.

WESTERHEIDE, D.E. and WESTWATER, J.W. (1961). "Isothermal growth of hydrogen bubbles during electrolysis". *AIChE Journal*, **7(3)**, 357–362.

ZHANG, Z., LIU, W. and FREE, M.L. (2020). "Phase-field m odeling a nd s imulation o f g as b ubble coalescence and detachment in a gas-liquid two-phase electrochemical system". *Journal of The Electrochemical Society*, **167(1)**.

ZHAO, X., REN, H. and LUO, L. (2019). "Gas bubbles in electrochemical gas evolution reactions". *Langmuir*, **35(16)**, 5392–5408.

APPENDIX A

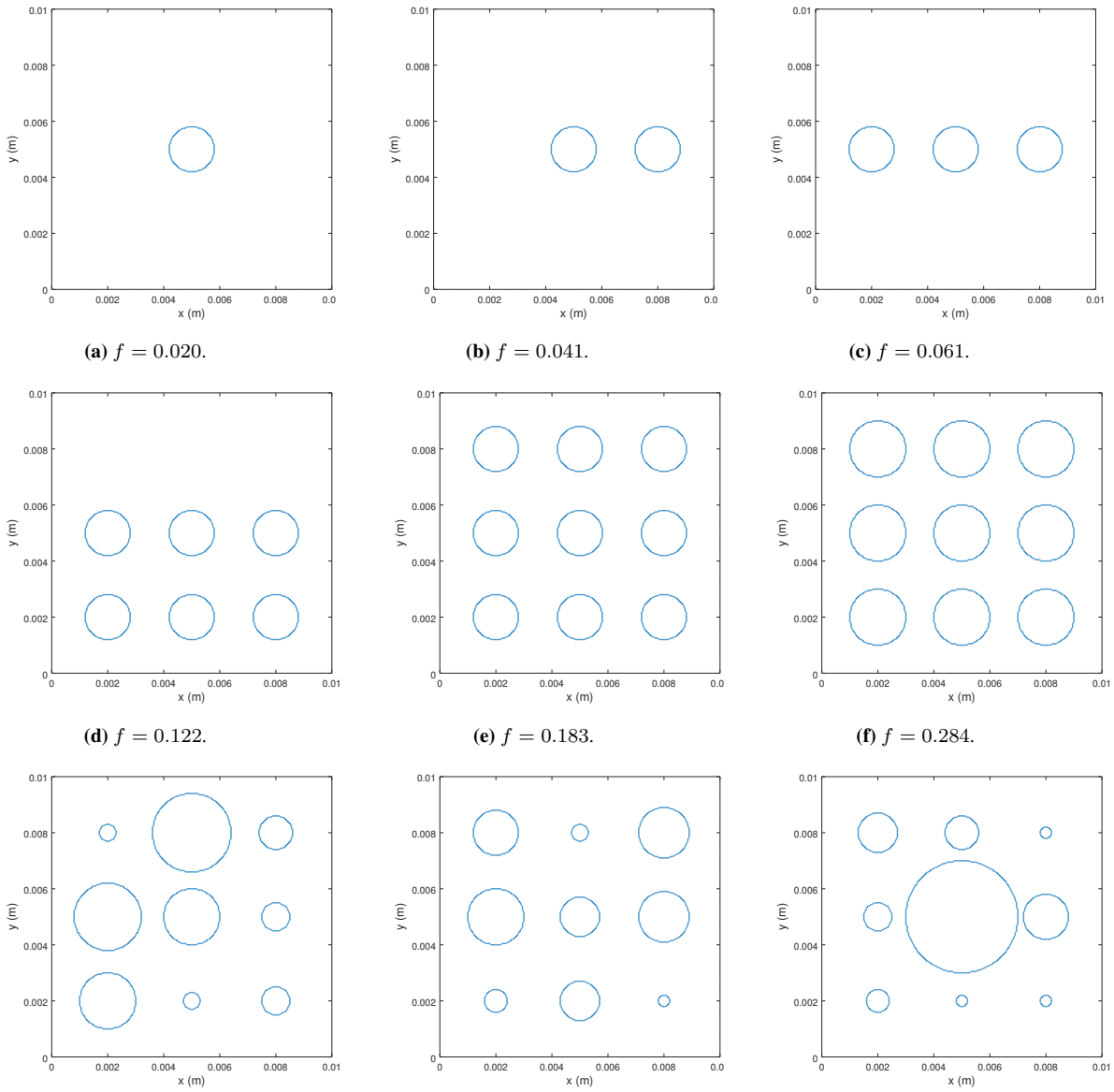

(a) $f = 0.020$. **(b)** $f = 0.041$. **(c)** $f = 0.061$.

(d) $f = 0.122$. **(e)** $f = 0.183$. **(f)** $f = 0.284$.

(g) $f = 0.203$. **(h)** $f = 0.143$. **(i)** $f = 0.190$.

Figure A1: The distribution of the 2D bubbles in the computational domain.

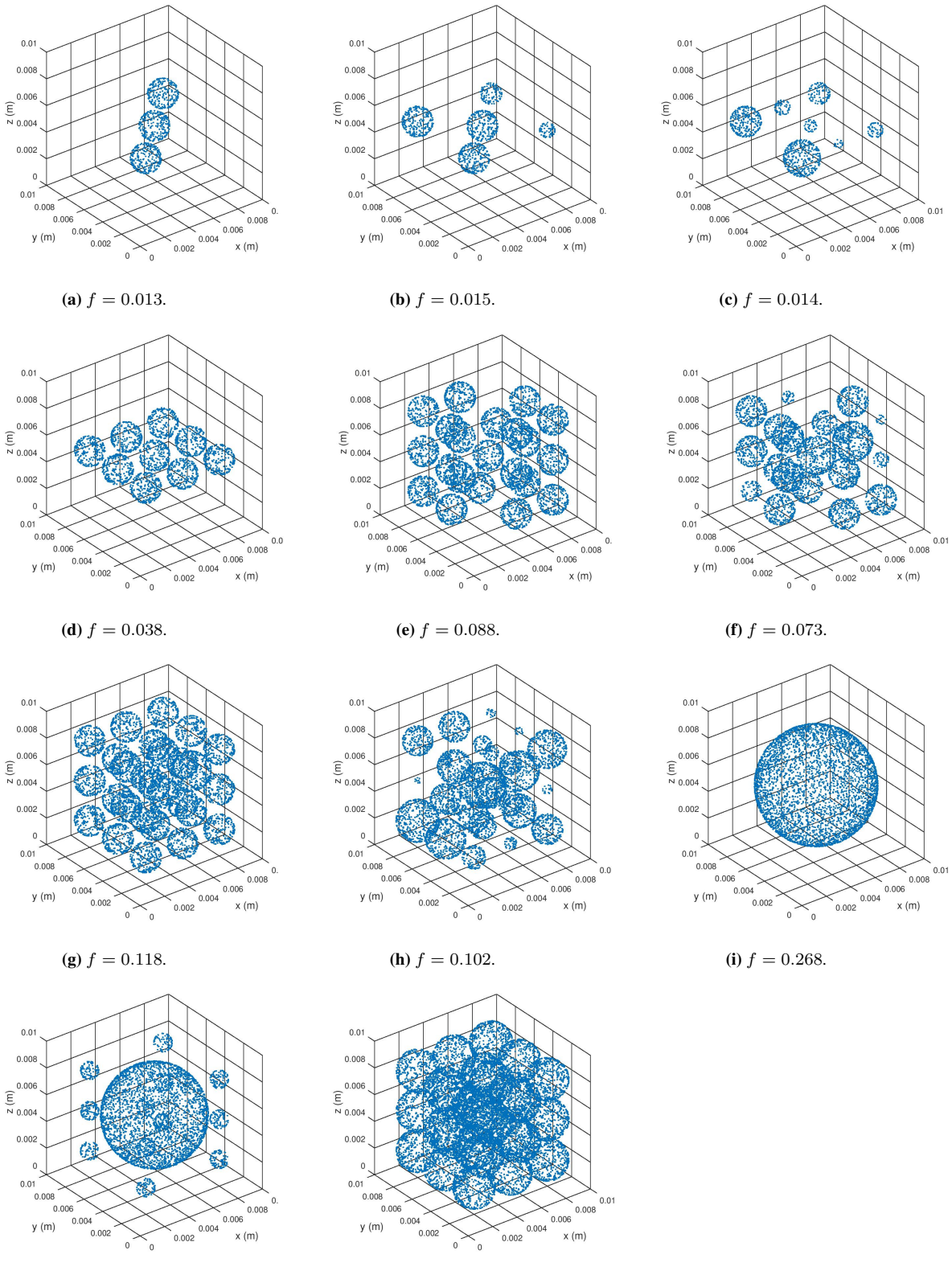

(a) $f = 0.013$. **(b)** $f = 0.015$. **(c)** $f = 0.014$.

(d) $f = 0.038$. **(e)** $f = 0.088$. **(f)** $f = 0.073$.

(g) $f = 0.118$. **(h)** $f = 0.102$. **(i)** $f = 0.268$.

(j) $f = 0.190$. **(k)** $f = 0.311$.

Figure A2: The distribution of the 3D bubbles in the computational domain.